

Full-scale testing of a novel slip control braking system for heavy vehicles

Leon Henderson, David Cebon¹

Cambridge University Engineering Department, UK

**Submitted to Proceedings of the IMechE, Part D: J. Automobile Engineering,
January 2015**

Response to reviewers' comments: 7 July 2015

Accepted for publication: 8 August 2015

Abstract

This paper summarises the measured emergency braking performance of a tri-axle heavy goods vehicle (HGV) semitrailer fitted with a novel pneumatic slip-control braking system developed by the Cambridge Vehicle Dynamics Consortium (CVDC). Straight-line braking tests were carried out from 40km/h in order to compare a commercially available electro-pneumatic HGV trailer ABS system and the CVDC system, which has bi-stable valves coupled with a sliding mode slip controller. On average, the CVDC system reduced stopping distance and air use by 15% and 22% respectively compared to conventional ABS. The most significant improvements were seen on a wet basalt tile surface (with similar friction properties to ice) where stopping distance and air use were improved by 17% and 30% respectively. A third performance metric, mean absolute slip error (MSE), is introduced to quantify each braking system's ability to track a wheel slip demand. Using this metric, the bi-stable valve system is shown to improve wheel slip demand tracking by 62% compared to conventional ABS. This improvement potentially allows more accurate control of wheel forces during extreme manoeuvres, providing scope for the future development of advanced stability control systems.

¹ Corresponding author:

Prof. David Cebon, Cambridge University Engineering Department, Trumpington Street, Cambridge, UK, CB2 1PZ.
Tel: +44 (0) 1223 332 665, Email: dc@eng.cam.ac.uk

Keywords

Anti-lock braking system, ABS, slip control, heavy vehicle, straight-line braking, brake system design, vehicle testing, pneumatic actuator, electro-pneumatic

Introduction and literature review

Motivation

In the UK, heavy goods vehicles (HGVs) were involved in 272 fatal traffic accidents in 2011. This equates to 8.4% of all fatal vehicle accidents. This is considerably higher than statistically expected, as HGVs only make up around 3% of the vehicle fleet [1, 2]. The Department for Transport estimate that preventing just one of these fatal accidents would result in £1.88 million in benefits [1]. In the US, one in nine traffic fatalities were found to involve a HGV in 2008 [3,4]. Of these accidents, rear-end collisions were the most common type (21%), followed by rollover (16%) [5].

The over representation of HGVs in fatal crash data can be attributed to several undesirable attributes of their dynamics. These include: rearward amplification during transient manoeuvres, lateral off-tracking [6] and their long emergency stopping distances. Even with the recent introduction of electronic braking systems (EBS) and the change from drum brakes to disc brakes, stopping distances of HGVs are typically 40% longer than those of passenger cars [7,8].

Anti-lock braking systems

Wheel-lockup during harsh braking manoeuvres is an event that can result in both increased stopping distances and loss of directional stability. In articulated vehicles, this loss of stability can result in jack-knifing or rollover. Anti-lock braking systems (ABS) have been developed for both passenger cars and heavy vehicles to prevent wheel-lockup occurring.

ABS systems on heavy vehicles operate on the same general principles as those used in passenger cars, the main difference being the use of pneumatics as opposed to the hydraulics [9]. Because pneumatic brake actuation is slow, the ABS systems used on heavy vehicles today cycle at only 1-2Hz, (compared to between 6Hz and 8Hz for passenger cars [9, 10]). A typical heavy vehicle ABS emergency stop on a wet road is shown in Figure 1. The ABS algorithm prevents wheel-lockup by releasing brake pressure when high-levels of wheel deceleration are sensed.

A vehicle state known as wheel slip, λ , is defined to represent the level of relative speed (i.e. the slip) between the tread band of the tyre and the road:

$$\lambda = \frac{v_x - R_r \omega}{v_x} \quad (1)$$

where R_r , ω and v_x are the rolling radius, angular velocity and longitudinal velocity respectively. Wheel slip varies between 0 and 1, where $\lambda = 0$ corresponds to freewheeling and $\lambda = 1$ corresponds to complete lock-up of the wheel.

The available adhesion force between the road and tyre (F_x) can be related to wheel slip. Sample adhesion-slip curves for dry asphalt and ice are shown in Figure 2 plotted using a model devised by Fancher [11]. As can be seen, the shape of the adhesion-slip curve can differ greatly depending on road conditions. The relationship is additionally dependent on variables such as vehicle speed, tyre inflation pressure, normal tyre load, as well as lateral slip. Although conventional ABS improves lateral stability by preventing lockup, its oscillatory nature means that the wheel slip varies periodically between low and high levels. Consequently, the peak braking force (highlighted in Figure 2) is not maintained throughout the braking event, resulting in sub-optimal straight-line braking performance.

Alternative braking strategies

‘Slip control’ is a broad term used to describe control strategies that have been developed as an alternative to ABS. In order to achieve the minimum possible stopping distance, an ideal slip controller would manipulate the braking torque so that wheel slip converges to the peak of the adhesion-slip curve. In order for a controller to identify this optimal slip point, the tyre force characteristics must be known or estimated. In reality a pre-set optimal slip value is often used, typically around $\lambda = 0.2$, to reduce computation requirements in the controller. More recent controller concepts fit adhesion-slip curves in real-time in order to estimate the optimal slip point for any operating conditions [12].

Researchers have investigated slip control using a range of different linear and non-linear control strategies on both passenger cars and HGVs [13-20]. In the case of HGV slip control, studies have predicted significant stopping distance reductions in simulation [20-22], however, only one study was found in which vehicle tests were performed [14]. In this study, a slip control strategy was implemented on a medium sized rigid HGV with an air-over-hydraulic braking system. In these tests, improved steerability of the vehicle was observed in

brake-in-turn scenarios. Straight-line-braking tests were also carried out. However, stopping distance comparisons to conventional systems were not made.

Miller et al [23] showed, through simulation, that slip control would only be advantageous on HGVs if fast acting, high flow rate pneumatic actuators were used. He predicted that a slip control system using pneumatic valves with a 3ms switching delay and 8mm diameter orifice (compared to 20-40ms, 8mm conventional pneumatic ABS modulator valves) could reduce stopping distances by up to 30% compared to conventional ABS [23]. Like many of the existing slip controller designs, Miller's required accurate measurements of the absolute longitudinal speed of the vehicle and individual braking forces. As these are not measured directly on commercially available vehicles, they would need to be obtained using state estimation techniques.

Novel brake actuators for improved control bandwidth

Many researchers have investigated completely replacing pneumatic and hydraulic brake components with electrical actuators [10, 24-27]. Siemens have presented working prototypes of an electro-mechanical wedge-brake concept. Siemens claim these brakes have one-tenth the energy expenditure of conventional hydraulic brakes [27]. Separate simulations carried out by Emereole [10] suggest that using electromechanical actuators on a passenger car could reduce stopping distances by approximately 10% on low friction roads. These benefits, however, were only seen when the conventional ABS control algorithm was replaced with a slip controller. Electromechanical brake systems have also been proposed for heavy vehicles [28, 29]. Haldex Brake Products carried out a range of straight-line braking tests using a 'bob-tail' tractor unit fitted with their own prototype electromechanical disc brake. Reductions in stopping distances of up to 24% on low friction roads were seen when compared to a conventional EBS, ABS system (where electric signals are used to communicate the brake pressure demand from the driver to electro-pneumatic regulator valves) [29]. These trials once again included the use of a slip controller as opposed to the conventional ABS algorithm.

The Cambridge Vehicle Dynamics Consortium (CVDC) has recently developed a high-speed bi-stable pneumatic valve for use in an electro-pneumatic braking system [21]. This valve is an order of magnitude faster than existing heavy vehicle ABS modulator valves and comparable to electromechanical brake designs, which can adjust to small changes in brake torque demand within 10ms [27]. A schematic of the CVDC valve is shown Figure 3. The valve includes a cantilevered steel flexure which is mounted between two permanent

magnets. Electrical pulses in a wire coil are used to switch the flexure from one pole-piece to the other. The low moving mass of the flexure and its high stiffness allow the valve to switch in approximately 3ms. The CVDC valve design has an 8mm diameter orifice and can therefore be used directly in-line (as opposed to the indirect piloted diagram valve system used in conventional pneumatic ABS modulator valves). Recent hardware-in-the-loop (HiL) experiments using a HGV disc brake assembly fitted with a load cell (to measure clamping force at the brake disc) and prototype bi-stable valves, controlled using Miller's sliding mode slip controller, have achieved reductions in stopping distance of up to 25% compared to a commercially available HGV ABS system [21].

Slip control using bi-stable pneumatic modulator valves

In this paper, the slip control strategy presented by Miller et al. [12] is implemented on a full-scale HGV trailer using prototype bi-stable, fast-acting pneumatic valves (developed from the earlier valve design presented by Miller et al. [21]).

The relevant slip control equations are presented briefly in this section, for further detail relating to controller derivations and the mechanical design of the bi-stable valves, readers are referred to the following publications [12, 21, 30].

Sliding-mode slip control system overview

Miller's slip control system can be simplified into the flow diagram shown in Figure 4. A pressure control loop is cascaded within a slip control loop, which tracks a prescribed wheel slip demand, λ_{dem} . As is shown in the figure, some state estimation is required to identify the adhesion force at the contact patch (F_x) and longitudinal vehicle speed (v_x). In addition to this, parameters such as the rolling radius of the tyre (R_r) and the brake gain (K_{BG}) must be known.

A first-order sliding surface (s) is defined as:

$$s = \lambda - \lambda_{dem} \quad (2)$$

where λ_{dem} is the demanded slip level. λ_{dem} was set to the estimated peak of the adhesion-slip curve in this study Table 1. Combining the sliding surface definition (Equation 2) with the equations of motion of a simplified single-degree-of-freedom model of a rolling wheel subject to a braking torque, $T_B = P_c K_{BG}$ (where P_c is brake chamber pressure and K_{BG} is brake gain), and following the sliding mode controller derivation in [31], gives the following expression for brake chamber pressure demand (P_{dem}):

$$P_{dem} = \frac{R_r R_b F_x - (1 - \lambda) \dot{v}_x J}{K_{BG} R_r} - k_s \left\{ \frac{s}{|s| + \delta} \right\} - \Phi_s s \quad (3)$$

where k_s , Φ_s and δ are tuneable gains, J is the rotational inertia of the lumped wheel-tyre mass, and v_x is vehicle speed. A differentiation is made here between R_r (the rolling radius) and R_b the radius through which the braking force acts.

Two bi-stable valves are used to modulate the brake pressure at each wheel. These are arranged in an inlet and outlet configuration (as shown in Figure 3). Pulse width modulation (PWM) is used to control the air flow through each of the valves. A simple proportional pressure controller is used to define the desired PWM mark-space ratio (R_{MS}) for the inlet and outlet valves, using the following relationship:

$$R_{MS} = k_p (P_{dem} - P_c) \quad (4)$$

where positive R_{MS} values corresponded to an inlet valve demand, with negative R_{MS} corresponding to an outlet valve demand. k_p is a tuneable gain and was set to $1.5 \times 10^{-5} \text{Pa}^{-1}$ for the CVDC bi-stable valves used in this work. This value was selected by Miller et al. [21] to achieve a control bandwidth larger than the expected wheel-hop frequency (12.5Hz). A 0.05bar deadzone was also included to prevent limit-cycling (see Miller³² for thorough limit-cycling analysis).

Sample simulation results of the slip control system discussed above with two different valve models, one corresponding to conventional ABS valves (20ms switching delay) and the other representing the prototype bi-stable valves (3ms switching delay), are shown in Figure 5a and Figure 5b respectively. The non-linear quarter vehicle and the actuator model used in these simulations are the same as those presented by Miller et al. [21]. As can be seen in Figure 5a, the wheel speed and slip traces for the slip controller using conventional ABS hardware (but using the slip-control strategy) are oscillatory throughout the stop. This is due to the low control bandwidth of these valves. By contrast, the bi-stable 3ms valves can theoretically track the peak of the slip curve for the majority of the stop (Figure 5b).

Performance metrics

Preliminary tuning of the main slip control loop was discussed in previous simulation studies [12, 21, 30]. Two performance metrics were used in these simulations: stopping distance and air consumption.

Stopping distance can be easily measured in both simulation and field tests. It provides a quantitative measure of how well the available adhesion is utilised by different systems on the same surface. Stopping distance (along with mean fully developed deceleration) is used in European and US legislation to specify minimum braking requirements for road vehicles [7, 33].

Air consumption increases as the brake system performs more ‘fill and exhaust’ cycles and therefore provides a measure of controller action. The amount of air available to the braking system is limited by the size of the air reservoirs on the vehicle. A system that uses considerably more air than existing systems would therefore be undesirable as it would require larger, heavier air tanks to be fitted to the vehicle.

Mean absolute slip error (MSE) is introduced in this work as a third performance metric. MSE is defined as follows:

$$MSE = \frac{1}{N} \sum |\lambda - \lambda_{dem}| \quad (5)$$

where N is the total number of data points.

MSE is used to quantify how well a slip controller can track a specified wheel slip level. This metric is applicable to stability control systems, where a precise braking force (requiring a specific slip level) may be demanded from individual wheels.

Stopping distance, air use and MSE values are displayed on Figure 5a and Figure 5b for comparison. In this simulation case the difference in stopping distance between a slip controller with conventional ABS hardware and one with high-speed pneumatic valves is only 6.2%; the performance improvement in terms of slip point tracking is, however, highlighted by the MSE value, which is reduced by 56% when high-speed valves are used.

Air consumption and stopping distance are often displayed as a conflict plot, which can be used to visually compare the performance of different braking systems, and can be used to tune the various sliding mode controller gains. Figure 6 shows one such conflict plot for a simulated slip controlled stop with a sliding mode switching gain, k_s , ranging from 10kPa to 10MPa . As can be seen in Figure 6, as the controller gain k_s is increased, stopping distance is at first reduced and air consumption remains relatively constant. Beyond a certain level of k_s , however, improvements in stopping distance diminish and air consumption increases significantly. The preferred gain for the system is therefore selected at the ‘knee’ of this conflict plot (shown in the figure). The other slip control gains, Φ_s and δ , were found to have

less influence on stopping distance than k_s , and were fixed at constant values of 100kPa and 0.05 respectively throughout all of the simulation and experimental results presented in this paper. The ‘ideal stop’ test case shown in Figure 6 represents a braking event where the instantaneous adhesion-slip curve peak is followed perfectly throughout the stop. As can be seen in the figure, the simulated slip control system achieves a stopping distance very close to the ideal case.

System design for implementation on tri-axle semitrailer

A 12.5m tri-axle semitrailer was used as the test bed for the sliding mode slip controller and bi-stable pneumatic valve system (the ‘Slip Control’ (SC) system). A HGV trailer was used for this prototype installation, as opposed to a tractor unit or rigid truck, for the following reasons:

1. Trailers generally have more available space around their wheel stations, allowing easier mounting of prototype hardware and instrumentation.
2. Applying the trailer brakes only in a tractor-semitrailer combination significantly reduces the chance of jack-knife during straight-line braking (compared to braking the full combination).
3. A semitrailer was readily available to the authors that had a modern trailer EBS ABS system fitted. This braking system had been modified so that it could be activated via a laptop computer – this was used as a benchmark braking system for comparison.
4. Once commissioned, the SC system could be extended to the tractor unit for full tractor-semitrailer tests (a subject of future work).

The bi-stable valve design previously presented by Miller et al. [21] was modified before installation on the trailer. Design improvements included: reducing the valves’ overall electrical power requirements, increasing their maximum operating pressure to above 9bar and improving their reliability (specifically the valve seals and accompanying power electronics). New bi-stable modulator valve assemblies (housing both the inlet and outlet valves) were manufactured for each wheel station. As can be seen in Figure 7 and Figure 8, each modulator valve assembly was mounted to the axle, as close as possible to the brake chamber, in order to minimise propagation delays of the pneumatic signals. This arrangement differs significantly from that common to conventional trailer braking systems, where ABS valves are typically mounted on the trailer chassis, near the middle of the axle group. Figure 8

also shows that the axles on this particular test trailer were steered – this system remained locked in its central position during the work discussed here.

A failure mode and effect analysis (FMEA) was carried out to ensure the safety of the test vehicle setup. This analysis indicated that, due to bi-stable nature of the valves, the prototype valve system could not be easily arranged such that it would always fail in a safe, predictable, manner. The chosen system was therefore installed in parallel to the conventional braking system, as shown in Figure 8. Shuttle valves fitted at each wheel station were connected to both braking systems, allowing the driver to override the SC system by applying the conventional foot-brake. A ‘3-2’ solenoid valve and pneumatic relay valves were also fitted upstream of the SC so that it could be isolated from the trailer’s air supply in the event of a failure. The local slip controllers shown in Figure 8 were mounted to the trailer chassis and housed the valve drive electronics as well as a microcontroller which performed the slip control and pressure control calculations. A schematic showing the functions carried out by the local controllers, and how they interfaced with the rest of the vehicle, is shown in Figure 9. Braking demands and vehicle states (such as vehicle speed and deceleration) were sent from a Matlab XPC computer in the tractor cab to the local slip controllers via CAN buses.

The conventional ABS system fitted to the vehicle included three Haldex EB+ generation 1 electronic control units (ECUs), as shown in Figure 8. Each ECU monitored two wheel speeds and included 2 pressure control channels. This layout is often referred to as a 6S-6M system as it senses 6 wheel speeds in total and has 6 pressure modulator channels. The system therefore allowed individual ABS control of each wheel. Brake pressure demands could be sent to the Haldex ECUs from the tractor by either the tractor’s foot-brake (via the standard pneumatic service brake connections), or from the XPC computer via a separate CAN bus.

Additional sensors and hardware

A VBOX II GPS logger (fitted within the tractor cab) was used to provide measurements of the following vehicle states:

- Position (longitude and latitude)
- Velocity
- Heading
- Acceleration (longitudinal and lateral)
- Distance covered since reset

As the GPS antenna was located on the roof of the tractor unit, its readings were affected by the movement of the suspended tractor cab. It was, however, still found to provide reasonable estimates of distance (for stopping distance calculations) in straight-line braking tests and longitudinal speed for slip control in the low-adhesion tests presented in this work.

Trailer reservoir pressure was measured using pressure transducers included within the Haldex EB+ brake ECUs on the trailer. These measured the line pressure at the ECU's reservoir connection. The trailer reservoirs were isolated from the tractor's compressor feed during braking tests via a manual valve. The change in reservoir pressure was then used to calculate the mass of air used during the stop using the following equation, which assumes adiabatic behaviour for the short duration tests [21]:

$$\Delta m_{air} = \frac{\Delta P_{Tank} V_{Tank}}{\gamma R T_{Tank}} \quad (6)$$

where Δm_{air} is the total mass of air used, ΔP_{Tank} is the change in tank pressure, V_{Tank} is the tank volume, T_{Tank} is the average tank temperature, R is the specific gas constant for air and γ is the ratio of specific heats for air.

Thermocouples were fitted to each brake disc to monitor brake temperature throughout the vehicle tests. Brake gain is known to vary with brake disc temperature, it was therefore necessary to run all braking tests in a specified brake temperature range in order to obtain reproducible results. Monitoring brake temperatures could also alert the test driver of potential brake overheating that could cause component damage.

Straight-line emergency braking comparisons

Straight-line braking tests were carried out at the MIRA testing facility, near Nuneaton, UK. A Volvo tractor unit (FH12, 6x2) provided by Haldex Brake Products Ltd was used to tow the test trailer presented in the previous section. Vehicle parameter values for the tractor-trailer combination are listed in Table 1. Wheel slip was calculated using wheel speed sensor signals and a velocity estimate from the VBOX GPS logger. Pre-processed adhesion-slip look-up tables were then used to estimate the magnitude of F_x in real time, for the current level of wheel slip. F_x , wheel slip and vehicle deceleration (once again measured using the VBOX logger) were passed to the main slip control equation (Equation 3) in order to calculate individual brake pressure demands (P_{dem}). Constant slip demands were sent to all

local wheel stations when slip control was active. These demands were chosen to approximately match the peak of the relevant adhesion-slip curve at 30km/h (8.33m/s).

Tests were carried out on three different wet surfaces. These were:

- ‘Delugrip’ (an asphalt surface with a nominal tyre/road adhesion coefficient of 0.75)
- ‘Bridport’ (a pebble surface with a nominal tyre/road adhesion coefficient of 0.40)
- ‘Basalt’ (a tiled surface with a nominal tyre/road adhesion coefficient of 0.30)

The adhesion coefficients quoted here are those supplied by MIRA as nominal values for passenger car tyres. It should be noted that those actually observed for the HGV trailer tyres used in this study were 23%, 30% and 60% less than nominal for wet Delugrip, Bridport and Basalt respectively (see μ_{peak} in Table 1).

Due to the limited length of the straight-line braking facility the initial speed of the braking tests was limited to 40km/h (11.11m/s) to prevent the vehicle over-running the end of the surface. All tests were carried out with the trailer unladen – this constituted a worst-case loading condition for the vehicle where substantial ABS cycling is expected on all common test surfaces. Only the trailer brakes were applied during these tests.

Brake gain measurement

Brake gain (K_{BG}) appears in the denominator of the main slip control equation (Equation 3) and, as was highlighted by Miller et al [12], can vary depending on the vehicle’s operating conditions. Miller showed through simulation that 20% errors in brake gain (which can be expected on a real vehicle) could substantially reduce the performance of the sliding mode slip controller.

In order to obtain brake gain estimates for the test vehicle, calibration tests were carried out on a rolling road dynamometer. The dynamometer (a Biesbarth MB 8000-S, located at MIRA) allowed one axle to be driven at a time while measuring the brake force (F_x) at each wheel. Tests were carried out on each of the three trailer axles at increasing brake pressures. The steady-state brake force at each wheel was recorded for each brake pressure and a first-order curve was fitted to the resulting dataset. The ensemble average results for all six wheels are shown in Figure 10. The first-order fit shown provides an estimate of the average brake gain (\bar{K}_{BG}) and P_{crack} (the lowest pressure at which a braking force is recorded), for all of the trailer wheels.

Closer analysis of the data indicated that there was some difference in brake gain (up to 15%) between wheel stations. The test data was therefore separated for each wheel, and curve fits were re-applied. These were uploaded to the individual slip controllers for the braking tests.

Adhesion-slip curve estimation

Constant-pressure braking tests from 40km/h (11.11m/s) were used to fit appropriate Fancher adhesion-slip models [11]. The total estimated force ($F_{x,total}$) for each test was calculated using the following equation:

$$F_{x,total} = \frac{v_{x,i} - v_{x,f}}{t_f - t_i} (m_{total}) - F_{aero} - F_{rolling} \quad (7)$$

where F_{aero} and $F_{rolling}$ are the aerodynamic drag and rolling resistance forces respectively; these were estimated at the required test speed using a separate coast down test [35].

Subscripts i and f correspond to initial and final data points respectively. Two seconds of data were used for each braking force calculation, with $v_{x,i}$ set to 30km/h (8.33m/s), 10km/h less than the initial brake application speed, to allow the vehicle to reach steady-state. Tests were repeated at increasing brake pressures until complete wheel lock-up was detected. $F_{x,total}$ was divided by the average slip levels of the braked wheels to obtain the adhesion-slip model for a single (average) wheel station at 30km/h (8.33m/s). The resulting adhesion-slip curves for all three test surfaces are shown in Figure 11.

Load transfer was taken into account by adjusting the individual normal tyre loads (F_z) (presented in Table 1) to give adjusted ‘dynamic’ values (\hat{F}_z), according to:

$$\hat{F}_z = F_z - \frac{F_x (m_{tractor} h_1 + m_{trailer} h_2)}{l_2 (m_{tractor} + m_{trailer})} \quad (8)$$

Equation 8 was derived from the simplified free-body diagram of a tractor semitrailer shown in Figure 12. Here, F_z is the static wheel load of an individual trailer wheel (obtained from vehicle weigh station data), $m_{tractor}$ and $m_{trailer}$ are the mass of the tractor and trailer respectively, h_1 , h_2 , and l_2 correspond to vehicle dimensions stated in Table 1 and F_x is the average adhesion force generated at each trailer wheel (noting that the tractor unit brakes were not activated during any of these tests). Equation 8 only applies to steady state braking and does not include transient pitching of the vehicle, tyre rolling resistance or aerodynamic drag.

Load transfer was estimated to reduce normal loads on the trailer wheels by 8% on the delugrip test surface, 4% on bridport and 2% on basalt tile (see Table 1). Peak tyre/road adhesion coefficients (μ_{peak}) were calculated for each surface using the corresponding ‘dynamic’ wheel loads (\hat{F}_z) and are also provided in Table 1. These values include a nominal $\pm 5\%$ tolerance to account for differences in adhesion along the test track, as seen in [36].

It should be noted that the tyre/road adhesion parameters in Table 1 represent average values, and were only applicable for the specific operating conditions of the vehicle; they did not take into account changes in parameters such as vehicle speed, lateral slip and variations in adhesion along the length of the test track. In future implementations of the SC system, these characteristics will need to be estimated online in real-time, e.g. using the methods described in [32].

Straight-line braking test method

The straight-line braking test procedure followed in this work differs slightly from the standard procedure described in United Nations Economic Commission of Europe’s (UNECE) Regulation 13 for measuring ABS performance. In the UNECE regulation, braking performance metrics are measured from when fully developed deceleration has been reached [33]; for the comparative tests carried out in this work it was seen as important to also include the initial signal delays and transient response of the braking system in the stopping distance calculations, as these could differ significantly between systems. The testing procedure followed for each individual straight-line braking test was as follows:

- 1.) Brake temperature check (tests only carried out if brake disc temperature was between 80°C and 120°C - repeated conventional ABS stops were used to warm up brake hardware and tyres)
- 2.) Braking system selected (conventional ABS or bi-stable ABS modulator valves), data logging commenced
- 3.) Air isolation valve closed (for air consumption measurement)
- 4.) Vehicle driven onto test surface at approximately 42km/h (11.67m/s)
- 5.) Clutch disengaged
- 6.) Vehicle allowed to coast to 40km/h (11.11m/s)
- 7.) Brakes automatically activated by ‘global controller’ computer at 40km/h (11.11m/s)
- 8.) Braking continued until vehicle reached stand-still
- 9.) Data logging stopped

10.) Air isolation valve opened (to recharge trailer reservoirs)

Repeated tests were performed with both braking systems on each surface. Slip control tests were carried out with increasing controller gains (k_s) to produce conflict plots of air consumption versus stopping distance, similar to that presented in Figure 6.

An upper limit for brake disc temperature of 120°C was recommended by Haldex, as brake fade typically begins beyond this point; making brake gain data potentially incorrect above this temperature. A lower limit of 80°C was also used in early test runs to ensure the tyres were warm. Data gathered from tests with initial brake disc temperatures less than 80°C were discarded.

Tests on each surface were performed on the same day, to reduce the effects of environmental conditions on test results. All surfaces were tested in the wet condition, using the water spray system that is part of the straight-line wet-grip facility at MIRA.

Straight-line braking test results

Results for each of the three test surfaces are summarized in Table 2 for both conventional ABS and the SC system. Results presented for the SC system represent switching gains (k_s) within the optimal range (minimizing both stopping distance and air use). Tests corresponding to controller gain values near the apparent optimal value were combined to ensure that at least 3 test runs were used to calculate each set of braking statistics. The average performance improvements achieved by the bi-stable valve system are also summarised in Table 2. Significant improvements were seen in all three performance metrics (stopping distance, air use and MSE) compared to the conventional HGV ABS system.

Figure 13 shows sample test results for conventional ABS and the SC system on the wet delugrip surface ($\mu_{peak}=0.58$). The oscillatory nature of the ABS can be clearly seen in this figure. The approximate peak of the slip curve ($\lambda=0.12$) is also shown on the wheel slip plots for both systems. The SC system is able to successfully control wheel slip around this point. The slip controller demands only small changes in brake pressure throughout the stop, whereas ABS has many full fill and exhaust cycles. This difference results in a reduction in air consumption for the SC system. The bottom subplots in Figure 13a and Figure 13b show the instantaneous adhesion utilisation of the wheel during the course of the stop. This represents the ratio of estimated adhesion force achieved (F_x) to the maximum adhesion force available (i.e. the slip curve peak). The SC system pressurises the brake chamber more quickly at the beginning of the event. This results in a more rapid rise in adhesion utilisation

than for the ABS system. The periodic drop in adhesion utilisation seen in Figure 13a during conventional ABS's exhaust cycles also contributes to the system's relatively long stopping distances.

Results of the wet delugrip tests are also presented in Figure 14, this time in the form of a probability distribution. This figure shows the proportion of time spent by the two braking systems at different levels of wheel slip, normalised by the time taken to stop the vehicle. The area under any section of this figure represents the proportion of time spent in that wheel slip range. The approximate peak of the adhesion-wheel slip curve is also superimposed on this figure. The shapes of the wheel slip distributions for both systems are relatively similar, but the SC system has a narrower, taller distribution, centred about the approximate slip curve peak, indicating that the system spends more time in this slip range compared to conventional ABS.

Figure 15 shows sample test results for the wet basalt tile surface ($\mu_{peak}=0.12$). The low level of adhesion on this test surface is similar to that of ice. Conventional ABS clearly struggles on this surface, with the brake chamber pressure regularly dropping to atmospheric pressure (noting that the pressures shown in Figure 15 are absolute). The adhesion utilisation can be seen to drop to 0% during these parts of the ASB braking cycle. In contrast the adhesion utilisation of the SC system is consistently near 100% for the first half of the stop. This difference is also obvious in the large stopping distance reduction achieved by the bi-stable valve system for this test case: 17% when compared to conventional ABS, as shown in Table 2. The MSE of the SC system for the wet basalt results (0.087) was higher than that observed for the other two test cases presented in Table 2: 0.057 and 0.062 for delugrip and bridport respectively). The low chamber pressures required for the wet basalt surface may partially explain the reduction in slip tracking performance. As can be seen in Figure 15b, the brake chamber pressure required equated to around 2 bar absolute pressure; this was lower than the chamber pressures used to tune the pressure control loop in previous studies (which involved tests centred around 4 bar absolute pressure) [21]. Because of this, the chamber pressure often overshoot the demand pressure; resulting in a subsequent overshoot in wheel slip (this can be seen in Figure 15b). Despite this observation, the performance improvements achieved on the wet basalt were still considerable; further tuning of the pressure control loop may provide scope to reduce stopping distances further in future tests.

Figure 16 once again shows the distribution of wheel slip throughout the stop – this time for a wet basalt test. This figure further highlights the difficulty conventional ABS has on this

surface. The distribution of wheel slip for ABS is very wide, and includes a peak close to $\lambda=0$, where adhesion force is low. The wheel slip distribution for the SC system on this surface is also wider than that seen for the same in Figure 14 (wet delugrip), however, it is considerably narrower than conventional ABS, spending much more time near the peak of the slip curve and considerably less time near $\lambda=0$.

A conflict plot of air use versus stopping distance for the wet basalt test results is shown in Figure 17. The reduction in stopping distance achieved by the SC system is obvious in this figure. The size of the markers used to represent the SC system results in this figure is proportional to the magnitude of the sliding mode switching gain (k_s). Simulation results for the same test case (taking into account the mass of the un-braked tractor, as stated in Table 1) are overlaid; as can be seen, the stopping distances predicted by the simulation model are very close to the experimental results. Air consumption is also similar for the lower gain settings, with some discrepancy at higher gains. A similar tuning pattern to that previously presented Figure 6 and in other publications [12, 21] can be seen in this figure (as indicated by the superimposed arrow).

The overall percentage improvements achieved by the SC system (15% reduction in stopping distance, 22% reduction in air use and 62% reduction in MSE) are encouraging. The stopping distance improvements were, however, slightly less those predicted in previous hardware-in-the-loop studies on a similar system. In [21] the improvement in stopping distance was predicted to be 23% for an icy surface, 6% better than that achieved in the wet basalt vehicle tests summarised in Table 2. As has already been mentioned, this difference may be attributed to the tuning of the pressure controller, which was overly aggressive. It may also be attributed to the one or more of the following factors:

- i) Slower controller operating frequency in vehicle tests compared to HiL controller (200Hz in vehicle tests; 500Hz in HiL tests).
- ii) Differences in initial vehicle speed.
- iii) Differences in tyre/road adhesion properties (lower adhesion coefficient in vehicle tests).
- iv) Lower normal tyre load in vehicle tests.
- v) Inaccuracies in adhesion force look-up table.
- vi) Imperfect knowledge of adhesion-slip curve peak value.

Some of these factors will be addressed in a follow-on project.

To investigate how the SC system performs at higher speeds, a small number of tests were performed from 60km/h (16.67m/s) to 42km/h (11.67m/s) on the basalt tile surface. Sample results from these tests are shown in Figure 18. At these higher vehicle speeds, the slip controller demonstrates significantly tighter slip point tracking than the 40km/h case summarised in Table 2; this is highlighted by the slip distribution in Figure 19. The MSE for this test was 0.05, almost 50% lower than that seen for the same system at lower speed. The adhesion utilisation plots shown in Figure 18 suggest that the SC system can consistently maintain the peak adhesion force throughout 60km/h (16.67m/s) to 42km/h (11.67m/s) speed range. It is hoped that, by introducing the bi-stable valve system to the tractor unit in future work, straight-line braking tests will be possible from 80km/h to a stand-still on the same MIRA wet basalt surface. These future tests will provide a further indication of what performance improvements can be achieved by the SC system.

It should once again be noted that, in these tests, GPS was used to provide a measurement of vehicle speed to the SC system. GPS is not suggested by the authors as a feasible means of vehicle speed measurement for a commercial SC system - it was used here simply to demonstrate the improvements that can be achieved through better control of wheel slip. Recent advancements in vehicle state estimation [32, 37] suggest that an accurate estimate of vehicle speed could be obtained using relatively low cost inertial sensors – such sensors are already present in modern vehicle motion control systems such as Electronic Stability Control (ESC). Integrating the SC system presented in this work with a vehicle speed observer could potentially allow a commercially viable system to be developed.

In this work, the brake gain (K_{BG}) at each wheel was measured using a rolling road dynamometer prior to the straight-line braking tests. The brake gain incorporates friction conditions between the brake pad and disk, the radius at which the braking torque is applied and the mechanical advantage achieved through the brake calliper. The value of K_{BG} could vary significantly depending on the operating conditions of the vehicle. In a commercial system this parameter would, therefore, need to be estimated during normal driving. The authors' suggest using a brake pulsing method, similar to that demonstrated by Miller [32], to estimate K_{BG} in real-time.

Conclusions

- i) An HGV trailer braking system incorporating bi-stable pneumatic ABS modulator valves and a sliding mode slip controller was tested for straight-line emergency braking performance on low adhesion surfaces.
- ii) The system was found to reduce stopping distance, air consumption and mean absolute slip error by $15\pm 2\%$, $22\pm 9\%$ and $62\pm 3\%$ respectively, relative to an existing HGV trailer ABS system.
- iii) Improvements seen in stopping performance metrics could allow HGVs to meet tighter legislation in the future. Reductions in air use could also allow smaller air reservoirs to be used on HGVs.
- iv) Improvements in mean absolute slip error suggest that the bi-stable valve slip control system could allow other vehicle-wide control systems (such as electronic stability control) to more accurately control the adhesion force at each wheel.

Future work

Work has now commenced to fit a 4x2 tractor unit with the CVDC slip control system. Further straight-line braking tests will be carried out in early 2015 using this tractor unit and the semitrailer already fitted with the braking system. Along with emergency braking tests, normal driving/braking performance will also be assessed to see if any reductions in air consumption and storage capacity can be achieved in everyday driving. The test vehicle will later be used to implement a combined braking and steering stability control system currently being developed by Morrison [38]. The performance of this system will be assessed using emergency lane change manoeuvres.

Acknowledgements

The authors would like to thank Jonathan Miller, Bob Prescott, Eddie Shaw and Larry Potter from Haldex Brake Products Ltd for their input and recommendations throughout the design stage of this project. The authors would also like to thank Gary Rogers and Ian Worrall (Haldex Brake Products Ltd), as well as technicians from MIRA and the Cambridge University Engineering Department, for their assistance during the vehicle installation and testing phase of the project.

This work was supported by Haldex Brake Products Ltd, the New Zealand Tertiary Education Commission and the Cambridge Vehicle Dynamics Consortium (CVDC). At the time of

writing the CVDC consisted of the following members: Anthony Best Dynamics, Camcon, Denby Transport, Firestone Industrial Products, Goodyear Tyres, Haldex Brake Products, MIRA, SIMPACK, SDC Trailers, Tinsley Bridge, Tridec, Volvo Trucks and Wincaton

Tables

Table 1. Vehicle parameter values and adhesion-slip model coefficients, straight-line braking tests, MIRA testing facility, Nuneaton, UK

Symbol	Parameter	Value	Source
h_1	Ground to hitch	1.17m	[39]
h_2	Ground to trailer centre-of-mass (unladen)	1.2m	[39]
l_1	Hitch to trailer centre-of-mass (unladen)	5.8m	[39]
l_2	Hitch to centre axle (trailer)	7.7m	[39]
l_3	Axle spacing (trailer)	1.43m	[39]
R_r	Wheel rolling radius (average, all trailer wheels)	0.528m	Calibrated against VBOX velocity signal
m_{tractor}	Tractor mass (combined sprung and unsprung)	9,400kg	Weigh station, MIRA
m_{trailer}	Trailer mass (combined sprung and unsprung, unladen)	11,700kg	Weigh station, MIRA
P_{crack}	Chamber pressure at which braking force becomes non-zero (average, all trailer wheels)	1.29bar	Rolling road dynamometer tests
F_z	Static normal load (individual trailer wheel, average)	14.9kN	Weigh station, MIRA
\hat{F}_z	Adjusted, ‘dynamic’ normal load calculated at peak adhesion-slip curve (individual trailer wheel, average)	Delugrip: 13.7kN Bridport Pebble: 14.3kN Basalt: 14.6kN	Equation 6.4
\bar{K}_{BG}	Brake gain (average, all trailer wheels)	1.80 kNm/bar	Rolling road dynamometer tests
C_0	Longitudinal slip stiffness (at zero slip, Fancher adhesion/slip model)	132.5kN	Calculated from normal wheel load, using relationship in ¹¹
V_f	Friction function shaping factor (Fancher adhesion/slip model)	Delugrip: 5m/s Bridport: 5m/s Basalt: 13.8m/s	Constant brake pressure tests
μ_{peak}	Peak tyre/road adhesion coefficient	Delugrip: 0.58±0.03 Bridport Pebble: 0.28±0.01 Basalt: 0.122±0.006	Constant brake pressure tests
μ_0	Coefficient of static friction (Fancher adhesion/slip model)	Delugrip: 0.80 Bridport Pebble: 0.30 Basalt: 0.125	Constant brake pressure tests
μ_f	Coefficient of dynamic friction (Fancher adhesion/slip model)	Delugrip: 0.5 Bridport Pebble: 0.20 Basalt: 0.112	Constant brake pressure tests

Table 2. Straight-line braking test performance summary, from 40km/h (11.11m/s) (percentages show relative change from conventional ABS)

	Metric	Conventional ABS	CVDC Slip Control
Wet Delugrip ($\mu_{\text{peak}}=0.58\pm0.03$)	Optimal sliding mode gain, ks (Pa)	N/A	50,000 - 70,000
	Number of tests	4	3
	Stopping distance (m)	Mean: 28.9 Max: 29.4 Min: 28.5	Mean: 25.5 (-12%) Max: 25.7 (-13%) Min: 25.4 (-11%)
	Air consumption (kg)	Mean: 0.049 Max: 0.051 Min: 0.048	Mean: 0.038 (-22%) Max: 0.051 (-0%) Min: 0.029 (-40%)
	MSE (unitless, calculated per test)	Mean: 0.13 Max: 0.15 Min: 0.12	Mean: 0.053 (-59%) Max: 0.060 (-60%) Min: 0.047 (-61%)
Wet Bridport ($\mu_{\text{peak}}=0.28\pm0.01$)	Optimal sliding mode gain, ks (Pa)	N/A	50,000 - 70,000
	Number of tests	8	7
	Stopping distance (m)	Mean: 54.8 Max: 56.1 Min: 49.7	Mean: 45.8 (-16%) Max: 46.7 (-17%) Min: 44.2 (-11%)
	Air consumption (kg)	Mean: 0.073 Max: 0.083 Min: 0.064	Mean: 0.062 (-15%) Max: 0.076 (-8%) Min: 0.045 (-30%)
	MSE (unitless, calculated per test)	Mean: 0.20 Max: 0.21 Min: 0.19	Mean: 0.068 (-66%) Max: 0.086 (-59%) Min: 0.048 (-75%)
Wet Basalt ($\mu_{\text{peak}}=0.122\pm0.006$)	Optimal sliding mode gain, ks (Pa)	N/A	50,000-70,000
	Number of tests	10	6
	Stopping distance (m)	Mean: 129 Max: 132 Min: 125	Mean: 107 (-17%) Max: 111 (-16%) Min: 104 (-17%)
	Air consumption (kg)	Mean: 0.133 Max: 0.140 Min: 0.127	Mean: 0.093 (-30%) Max: 0.115 (-18%) Min: 0.070 (-45%)
	MSE (unitless, calculated per test)	Mean: 0.21 Max: 0.22 Min: 0.20	Mean: 0.087 (-59%) Max: 0.090 (-59%) Min: 0.084 (-58%)
Average change relative to ABS (all Surfaces)	Stopping distance	baseline	-15±2%
	Air consumption	baseline	-22±9%
	MSE (unitless)	baseline	-62±3%

Figures

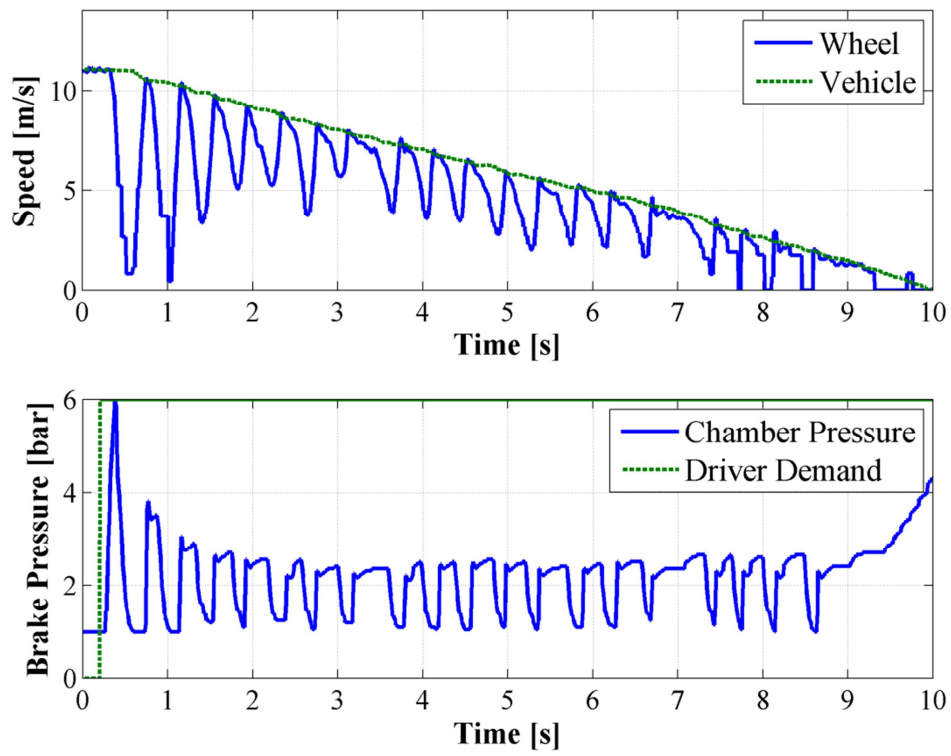


Figure 1. Heavy vehicle ABS performance on wet pebble surface ($\mu_{\text{peak}}=0.28$)

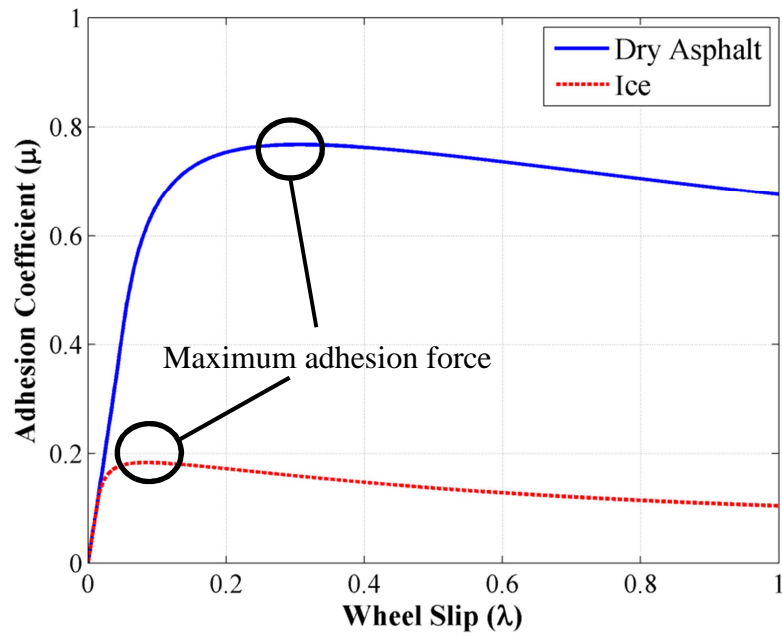


Figure 2. Sample adhesion-slip curves, showing slip-curve peak, plotted using the model presented by Fancher [11]

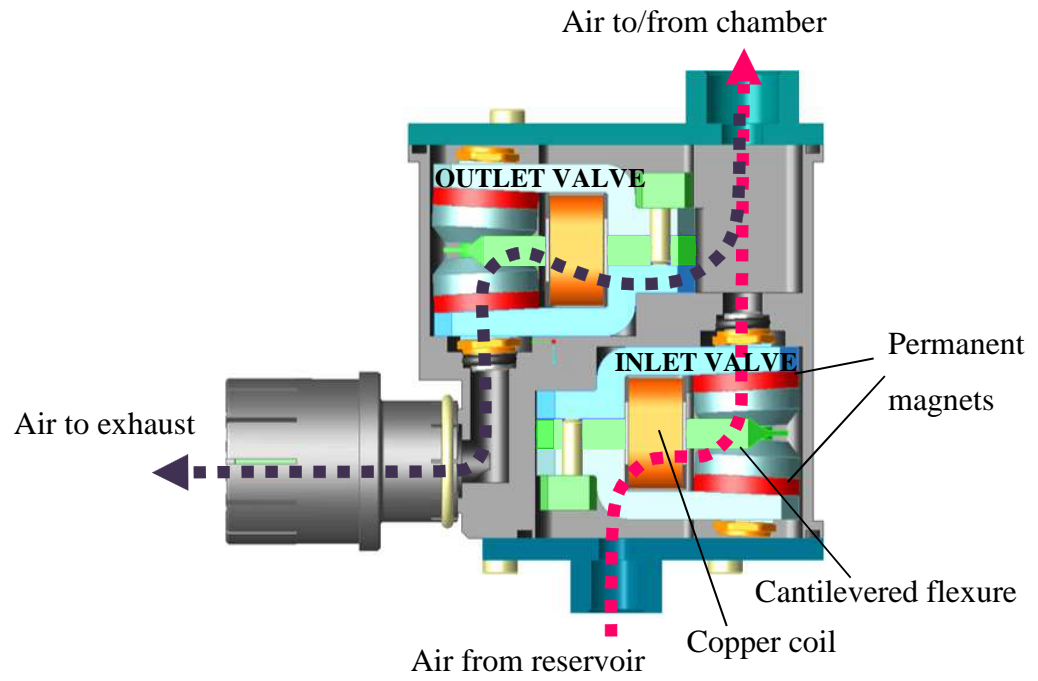


Figure 3. Cross-section of valve enclosure incorporating two CVDC bi-stable valves – used for brake pressure modulation

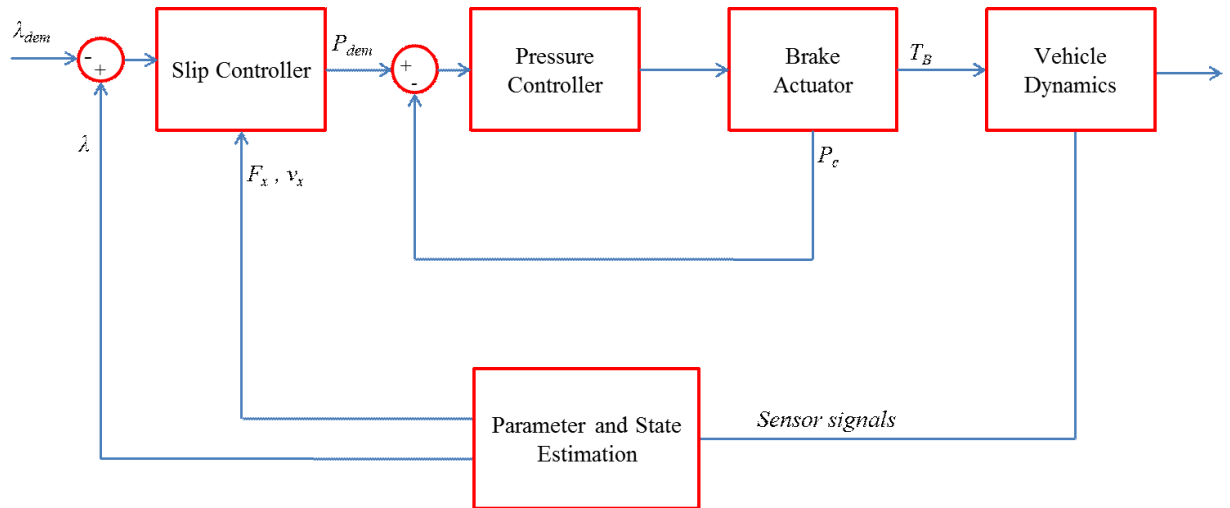
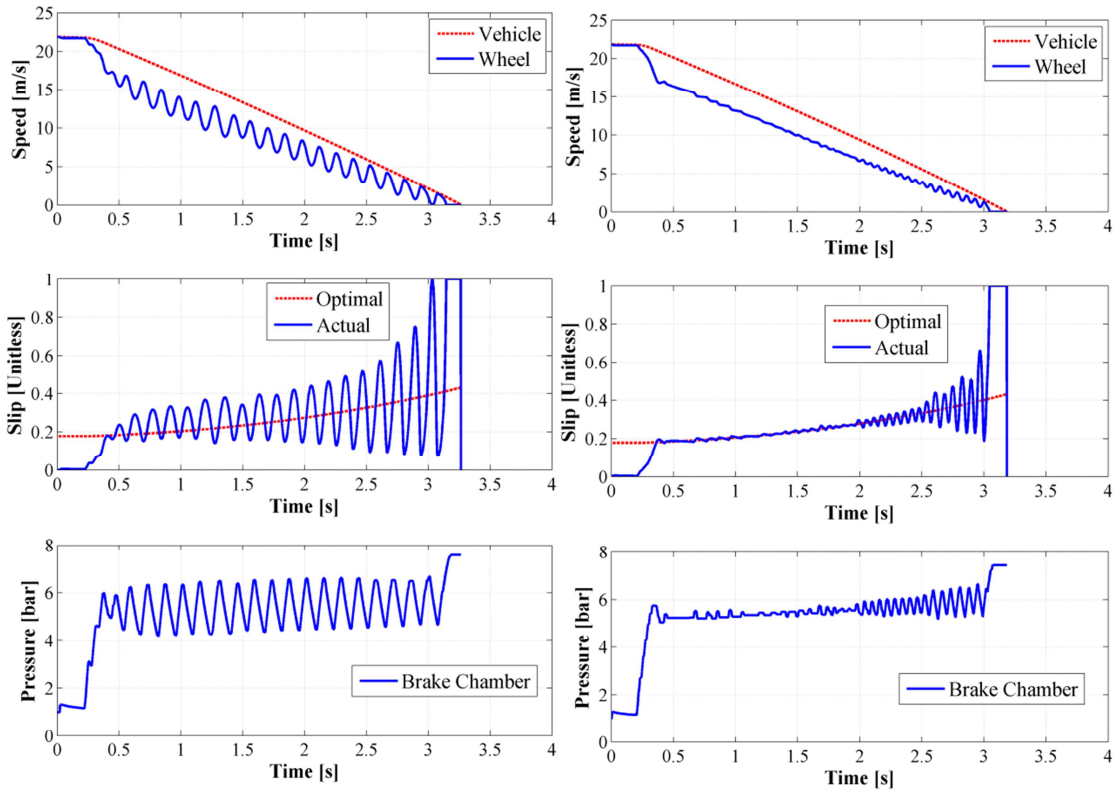


Figure 4. Slip control system flow diagram



Stopping Distance	37.3m
MSE	0.09
Air Consumption	0.046kg

(a)

Stopping Distance	35.0m
MSE	0.04
Air Consumption	0.017kg

(b)

Figure 5. HGV quarter vehicle braking simulation results - braking from 80km/h (22.22m/s) on a smooth, dry asphalt road; (a) Sliding mode slip controller with existing ABS modulator valves, (b) Sliding mode slip control with 3ms bi-stable modulator valves

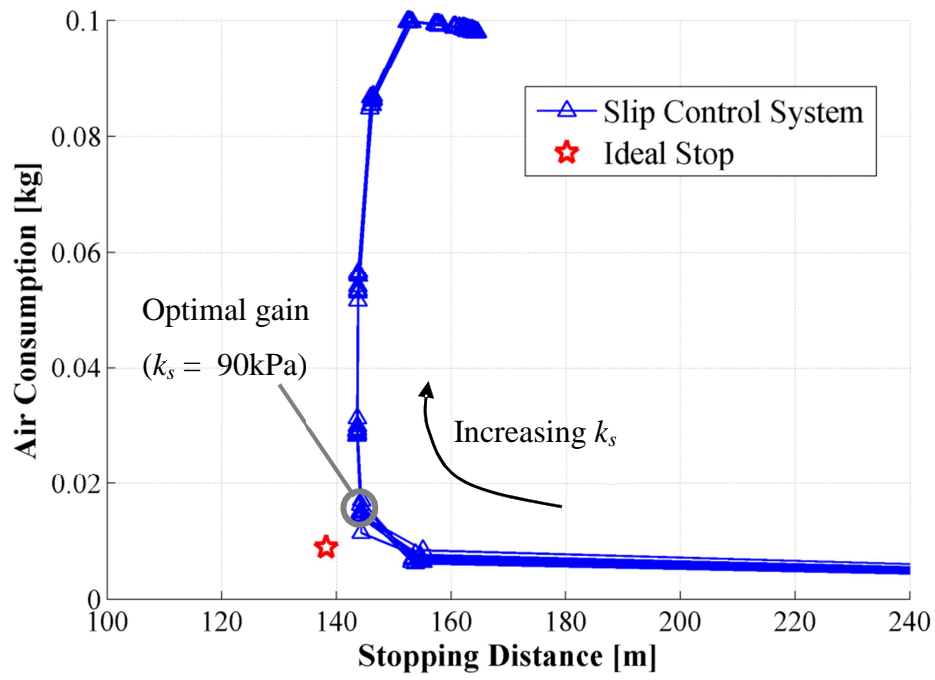


Figure 6. Conflict plot of simulated straight-line braking performance of sliding mode slip controller with 3ms bi-stable pneumatic valves on a smooth icy surface ($\mu_{\text{peak}}=0.2$), initial vehicle speed = 80km/h (22.22m/s)



Figure 7. Test vehicle and high-speed modulator valve installed at wheel end

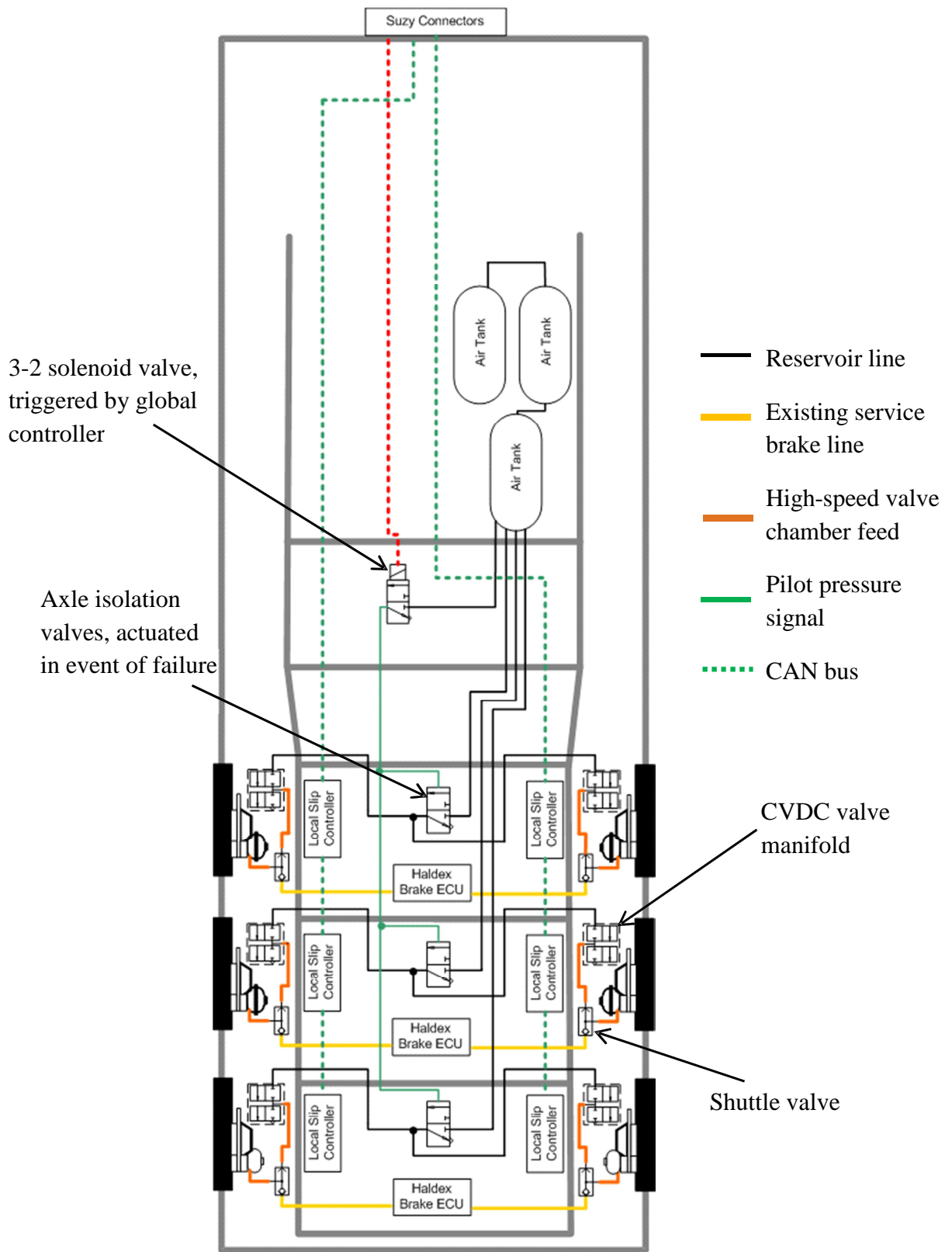


Figure 8. Slip control braking system fitted in parallel to existing Haldex setup for back-to-back braking tests (detail of existing Haldex system not shown) (not to scale)

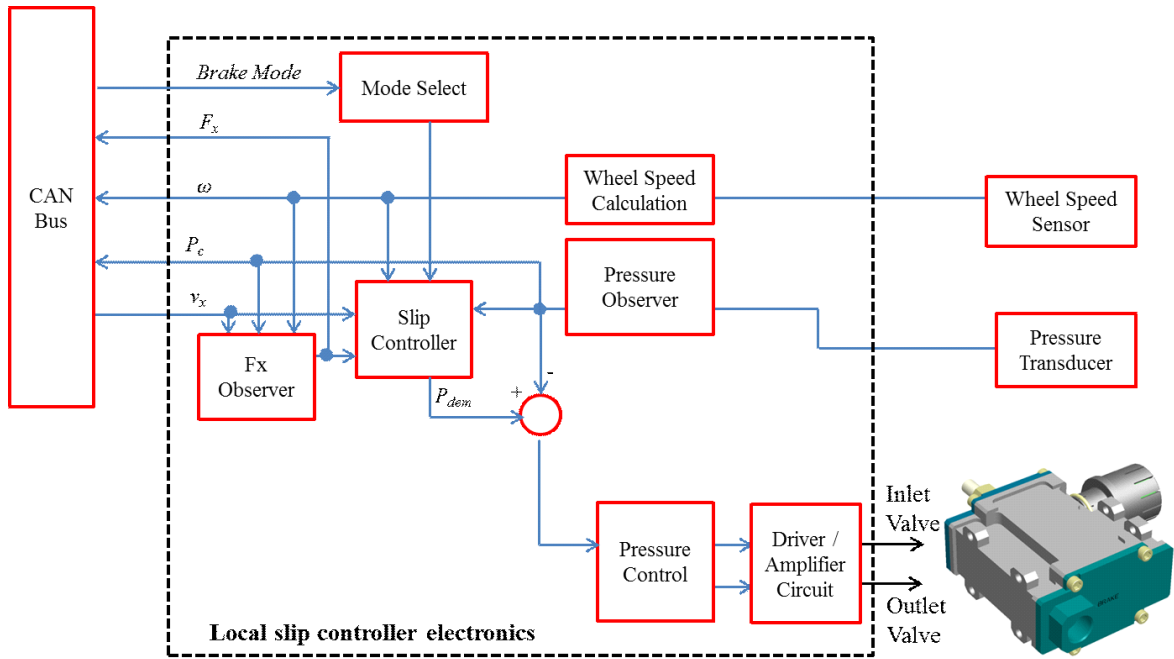


Figure 9. Local slip controller flow diagram

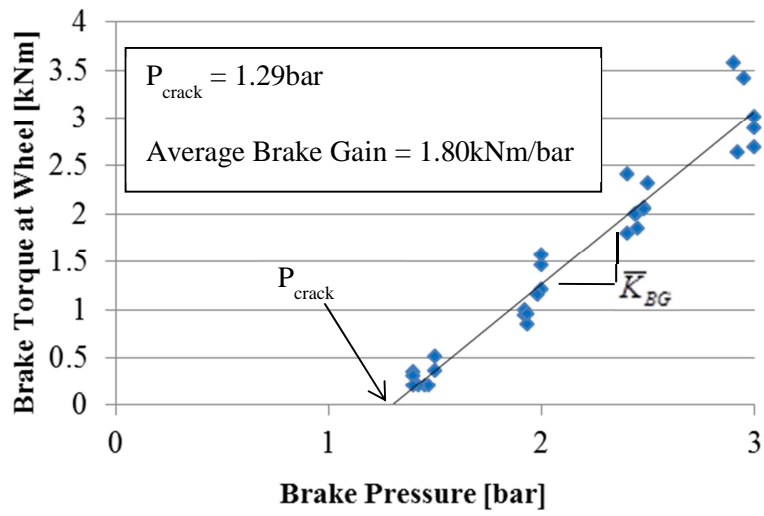


Figure 10. Rolling road dynamometer results and brake gain calculations, all trailer wheels

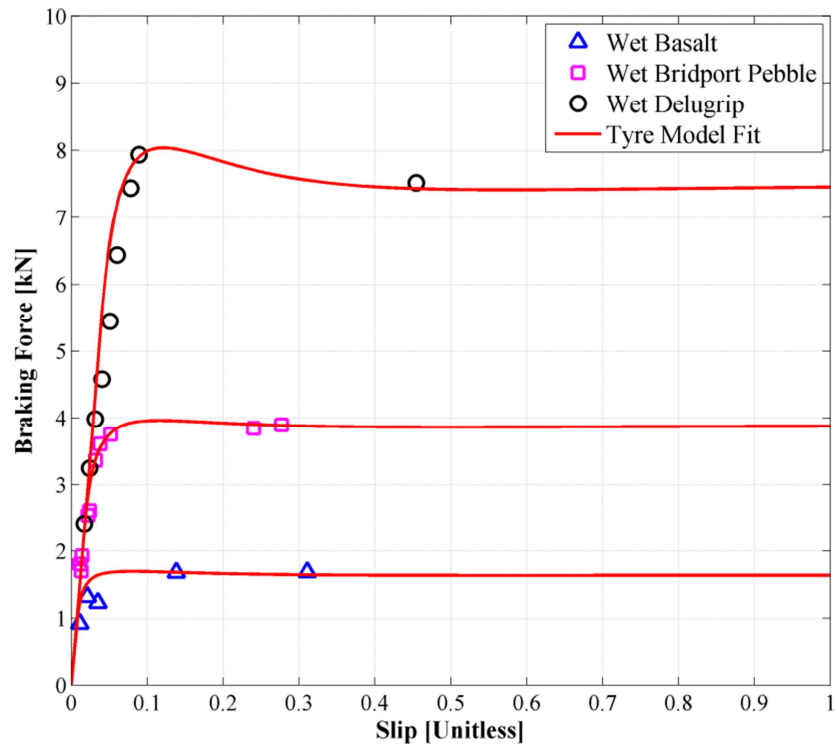


Figure 11. Adhesion force-slip curves [11] fitted against test results, 30km/h (8.33m/s), unladen

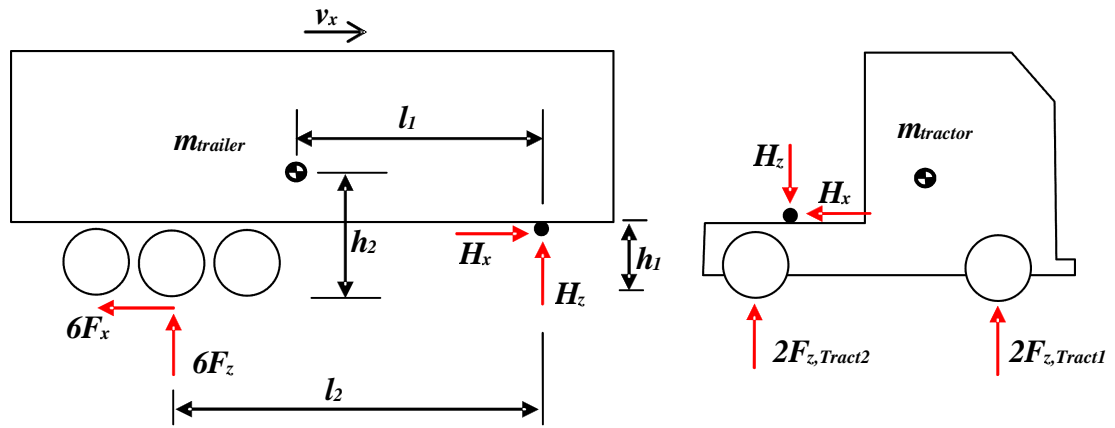
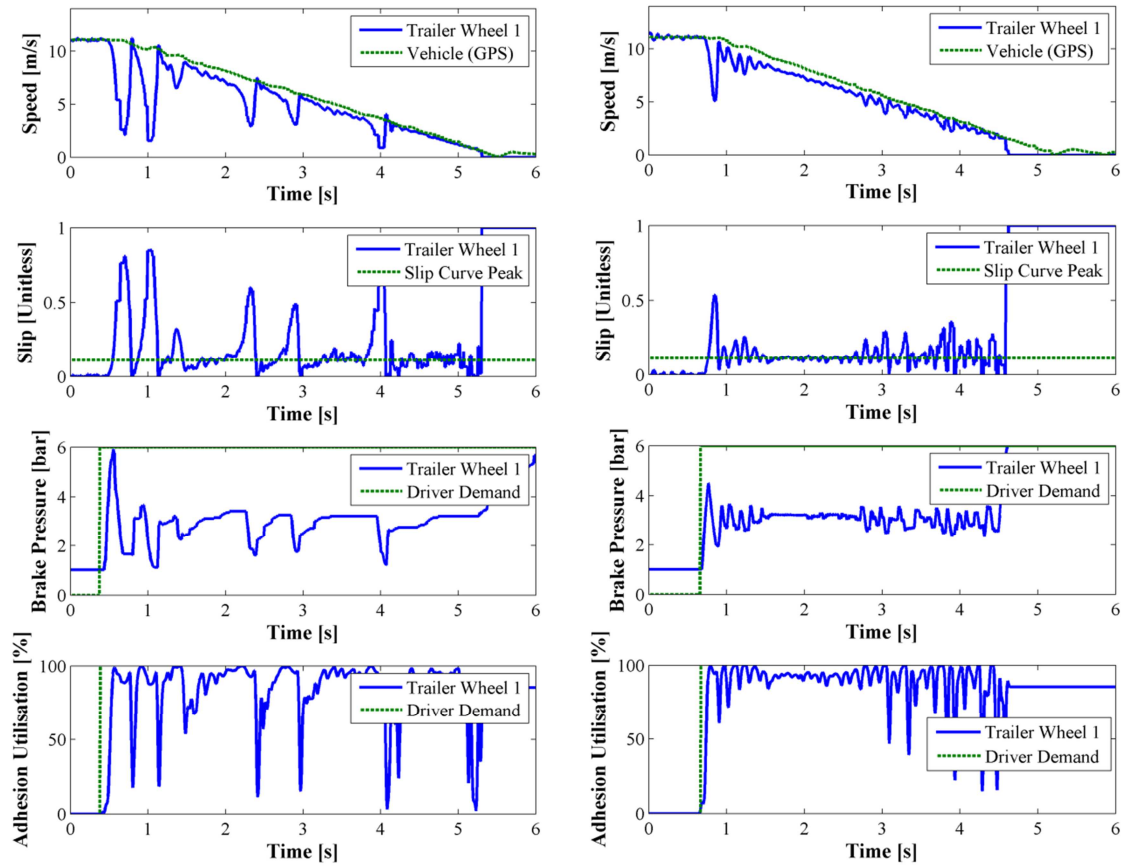


Figure 12. Free-body diagram for straight-line braking of tractor semitrailer combination used for dynamic load transfer calculations, tractor unit brakes disabled (corresponding inertial properties stated in Table 1).



Stopping Distance	28.9m
MSE	0.14
Air Consumption	0.049kg

(a)

Stopping Distance	25.4m
MSE	0.05
Air Consumption	0.035kg

(b)

Figure 13. Straight-line braking test results, wet delugrip ($\mu_{\text{peak}}=0.58$), braking from 40km/h (11.11m/s); (a) Conventional trailer ABS (6S-6M), (b) Slip control system

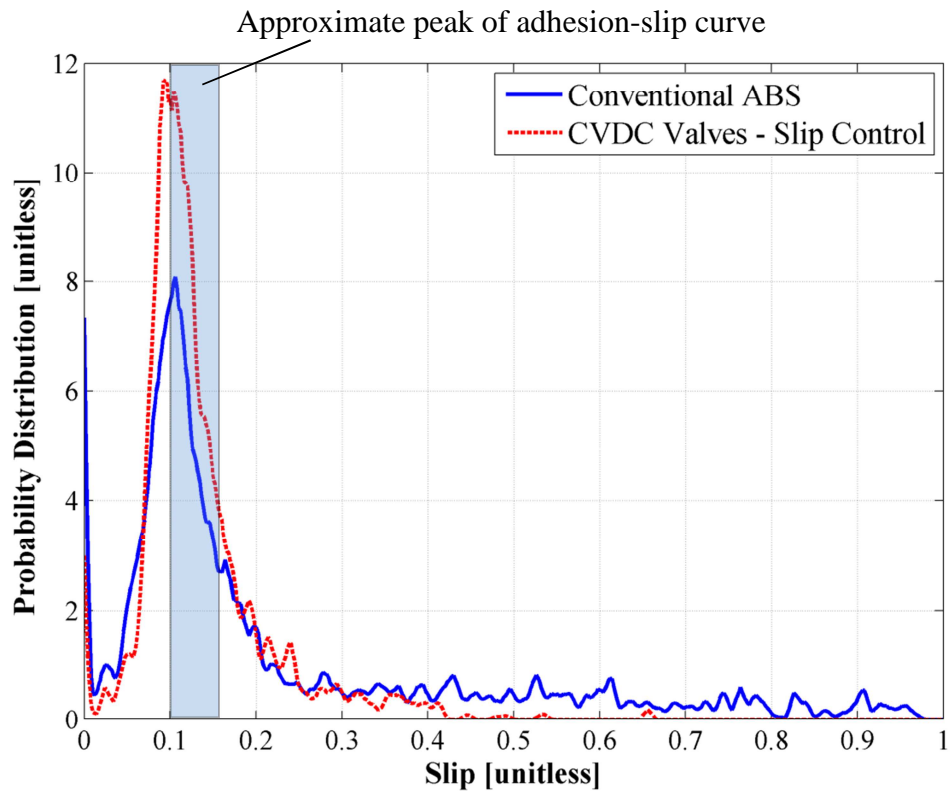
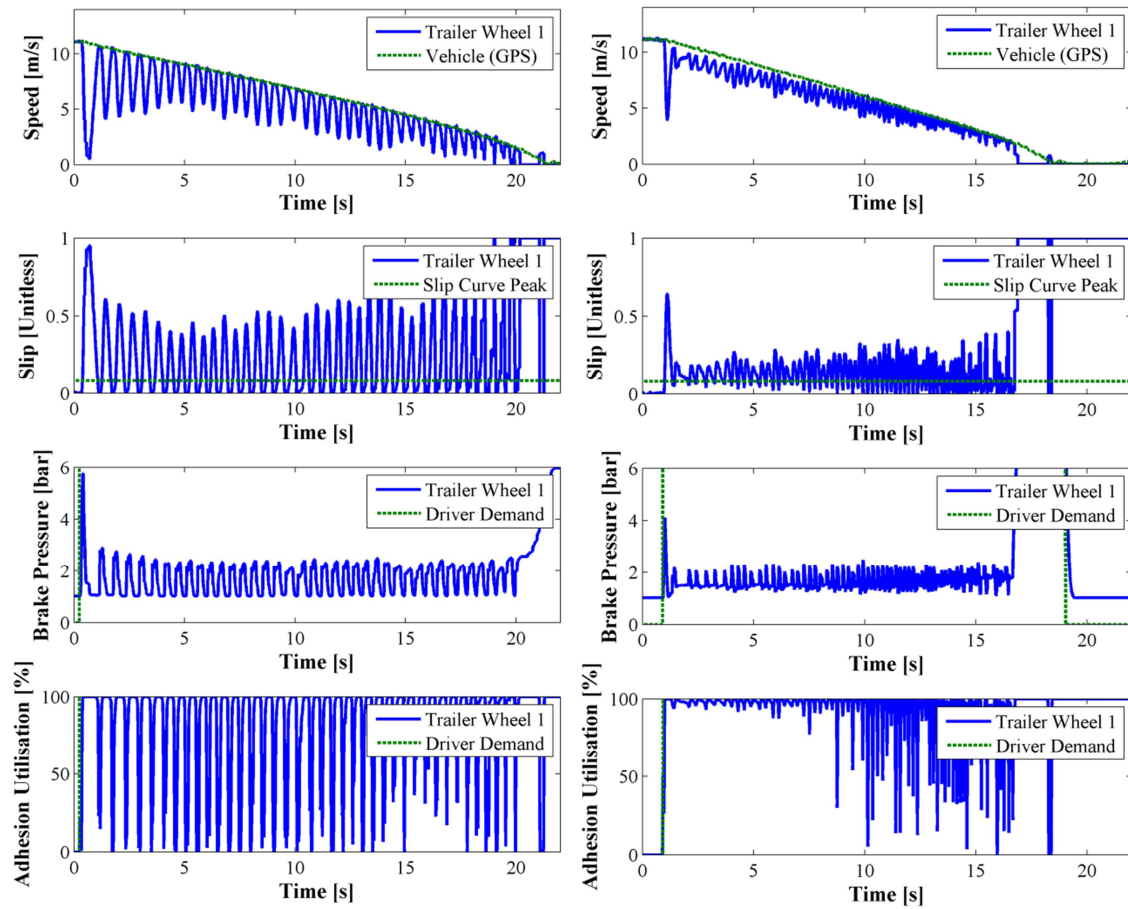


Figure 14. Probability distribution functions of slip error during braking event (all trailer wheels) - straight-line braking on wet delugrip ($\mu_{\text{peak}}=0.58$), from 40km/h (11.11m/s)



Stopping Distance	129m
MSE	0.23
Air Consumption	0.13kg

(a)

Stopping Distance	106m
MSE	0.09
Air Consumption	0.084kg

(b)

Figure 15. Straight-line braking test results, wet basalt tile ($\mu_{\text{peak}}=0.12$), braking from 40km/h (11.11m/s); (a) Conventional trailer ABS (6S-6M), (b) Slip control system

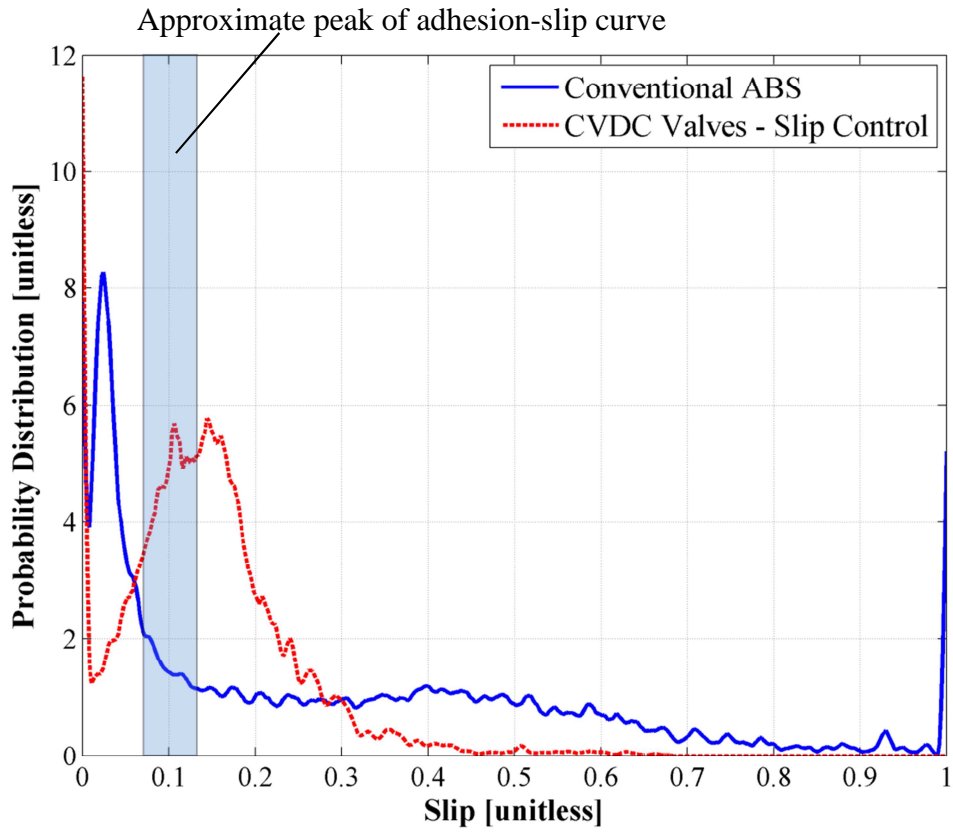


Figure 16. Probability distribution functions of slip during braking event (all trailer wheels) - straight-line braking on wet Basalt ($\mu_{\text{peak}}=0.12$), from 40km/h (11.11m/s)

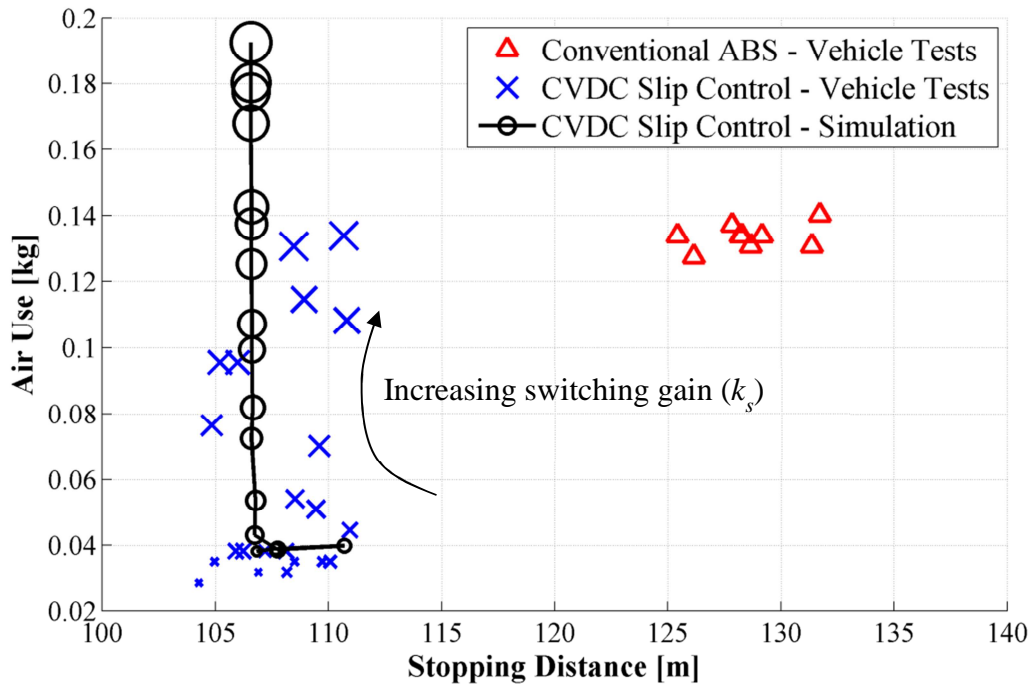
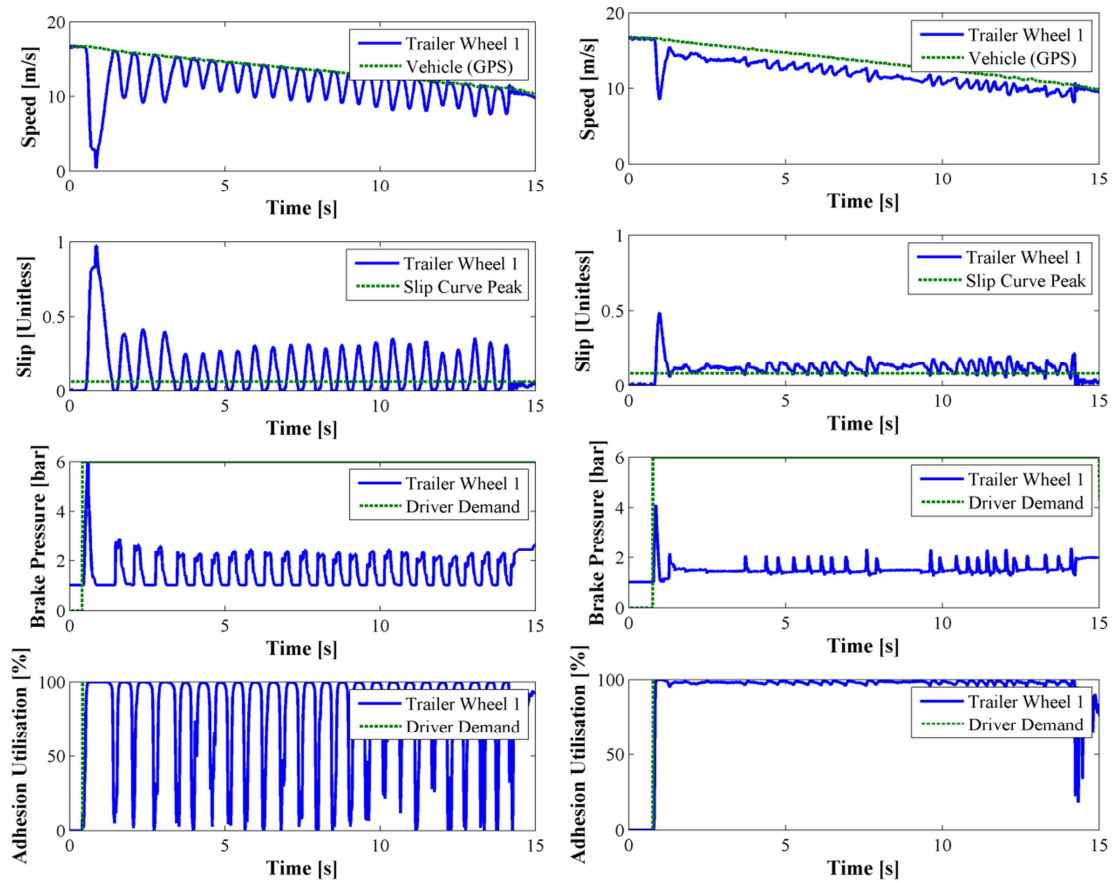


Figure 17. Conflict plot for straight-line braking test results – wet Basalt ($\mu_{\text{peak}}=0.12$), braking from 40km/h (11.1m/s), marker size proportional to controller gain (k_s)



Stopping Distance	171m
MSE	0.13
Air Consumption	0.11kg

(a)

Stopping Distance	156m
MSE	0.05
Air Consumption	0.035kg

(b)

Figure 18. Straight-line braking test results, wet basalt tile ($\mu_{\text{peak}} = 0.12$), braking from 60km/h (16.67m/s) to 42km/h (11.67m/s); (a) Conventional trailer ABS (6S-6M), (b) Slip control system

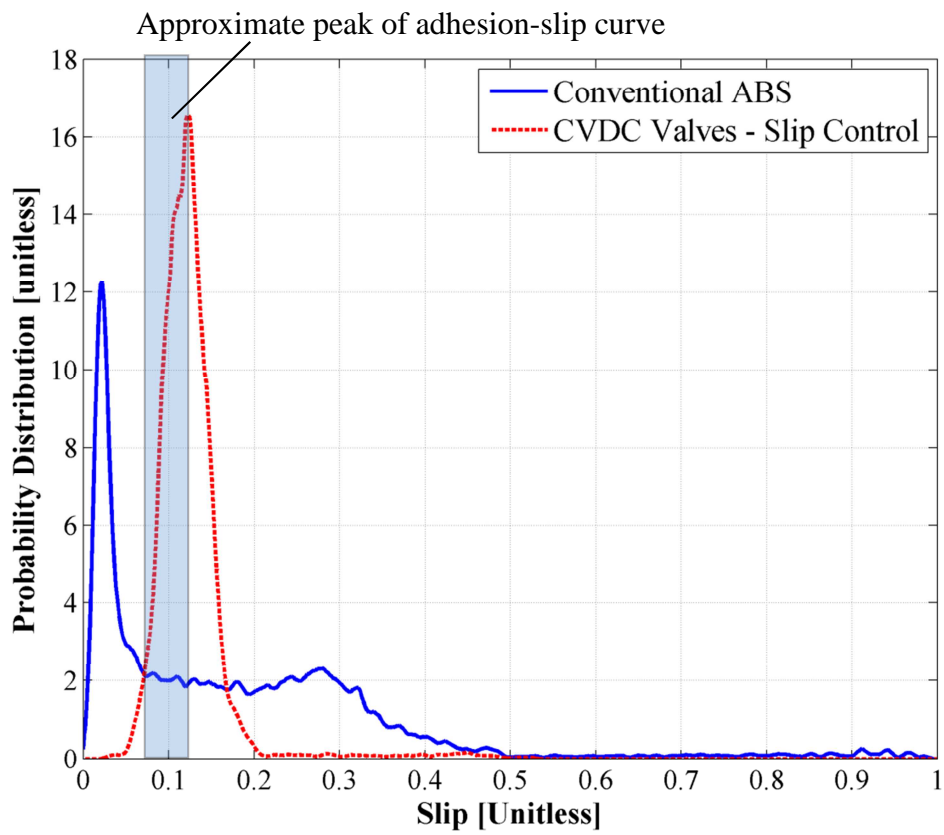


Figure 19. Probability distribution functions of slip during braking event (all trailer wheels) - straight-line braking on wet Basalt ($\mu_{\text{peak}}=0.12$), from 60km/h (16.67m/s) to 42km/h (11.67m/s)

References

1. Department for Transport. Road casualties Great Britain 2007. *Transport Statistics Publications*. Report, The Stationary Office, UK, 2008.
2. Department for Transport. Vehicles involved in reported road accidents (RAS20), *Road accidents and safety statistics*, <https://www.gov.uk/government/statistical-data-sets/ras20-drivers-riders-and-vehicles-in-reported-road-accidents#table-ras20007> (2011, accessed 10 January 2015).
3. Federal Highway Administration. Persons fatally injured in motor vehicle crashes. *Highway statistics 2007*. Report, Department of Transportation, USA, 2008.
4. National Centre of Statistics and Analysis. Large Trucks. *Traffic Safety Facts 2008*. Report no. 810989, 2009.
5. Jarossi L, Matteson A and Woodrooffe J. Trucks involved in fatal accidents factbook 2006. Report, The University of Michigan Transportation Research Institute, USA, 2008.
6. Jujnovich B, Odhams A, Roebuck R and Cebon D. Active rear steering control of a tractor-semitrailer. In: *International Symposium of Advanced Vehicle Control*, Kobe, Japan, 6-9 October, 2008, paper no. 097.
7. Dunn A and Hoover R. Class 8 truck tractor braking performance improvement study. Report, Department of Transportation, USA, 2004.
8. Forkenbrock G, Flick M and Garrot W. A comprehensive light vehicle antilock brake system test track performance evaluation. SAE paper 1999-01-1287, 1998.
9. Bosch. *Automotive handbook*. 5 ed, 2000.
10. Emereole O. *Antilock performance comparison between hydraulic and electromechanical brake systems*. Masters Thesis, University of Melbourne, Australia, 2003.
11. Fancher P. Generic Data for representing truck tire characteristics in simulations of braking and braking-in-a-turn maneuvers. Report, Great Lakes Center for Truck and Transit Research, USA, 1995.

12. Miller J and Cebon D. A high performance pneumatic braking system for heavy vehicles. *Vehicle System Dynamics*. 2010; 48: 373-92.
13. Kienhöfer FW and Cebon D. Improving ABS on heavy vehicles using slip control. In: *9th International Symposium on Heavy Vehicles, Weights and Dimensions*, Pennsylvania, 18-22 June, 2006.
14. Kawabe T, Nakazawa M, Notsu I and Watanabe Y. A sliding mode controller for wheel slip ratio control system. *Vehicle System Dynamics*. 1997; 27: 393-408.
15. Will A, Hui S and Zak S. Sliding mode wheel slip controller for an antilock braking system. *International Journal of Vehicle Design*. 1998; 19: 523-39.
16. Petersen I, Johansen TA, Kalkkuhl J and Ludemann J. Wheel slip control in ABS brakes using gain-scheduled constrained LQR. In: *Conference on Hybrid Control and Automotive Applications*, Berlin, Germany, 7-8 June, 2001.
17. Johansen TA, Petersen I, Kalkkuhl J and Ludemann J. Gain-scheduled wheel slip control in automotive brake systems. *IEEE Transactions on Control Systems Technology*. 2003; 11: 799-811.
18. Bauer M and Tomizuka M. Fuzzy logic traction controllers and their effects on longitudinal vehicle platoon systems. *Vehicle Systems Dynamics*. 1996; 25: 277-303.
19. Kimbrough S and Datla K. An effective means for implementing wheelslip control without a ground speed sensor. *Vehicle System Dynamics*. 1996; 25: 327-39.
20. Jiang F and Gao Z. An application of nonlinear PID control to a class of truck ABS problems. In: *IEEE Conference on Decision and Control*, Orlando, USA, 4-7 December, 2001.
21. Miller J, Henderson L and Cebon D. Designing and testing an advanced pneumatic braking system for heavy vehicles. *Proceedings of the Institution of Mechanical Engineers Part C-Journal of Mechanical Engineering Science*. 2013; 227: 1715-29.
22. Kienhofer F. Heavy vehicle wheel slip control. PhD Thesis, University of Cambridge, UK, 2011.

23. Miller J and Cebon D. An investigation of the effects of pneumatic actuator design on slip control for heavy vehicles. *Vehicle System Dynamics*. 2013; 51: 139-64.
24. Krishnamurthy P, Wenzhe L, Khorrami F and Keyhani A. Robust force control of an SRM-based electromechanical brake and experimental results. *IEEE Transactions on Control Systems Technology*. 2009; 17: 1306-17.
25. Xiang WD, Richardson PC, Zhao CM and Mohammad S. Automobile brake-by-wire control system design and analysis. *IEEE Transactions in Vehicle Technology*. 2008; 57: 138-45.
26. Balogh L, Strelci T, Nemeth H and Palkovics L. Modelling and simulating of self-energizing brake system. *Vehicle System Dynamics*. 2006; 44: 368-77.
27. Fox J, Roberts R, Baier-Welt C, Ho L, Lacraru L and Gombert B. Modeling and Control of a Single Motor Electronic Wedge Brake. SAE paper 2007-01-0866, 2007.
28. Palkovics L and Fries A. Intelligent electronic systems in commercial vehicles for enhanced traffic safety. *Vehicle System Dynamics*. 2001; 35: 4,227- 89.
29. Seglo F. Brake-by-wire on heavy truck. In: *Highly Automated Vehicles for Intelligent Transport*, Boras, Sweden, 21-22 June, 2011.
30. Miller J and Cebon D. Modelling and performance of a pneumatic brake actuator. *Proceedings of the Institution of Mechanical Engineers Part C-Journal of Mechanical Engineering Science*. 2012; 226: 2077-92.
31. Slotine J and Weiping L. *Applied nonlinear control*. Englewood Cliffs, New Jersey: Prentice Hall, 1991.
32. Miller J. *Advanced braking systems for heavy vehicles*. PhD Thesis, University of Cambridge, UK, 2010.
33. United Nations Economic Commission for Europe (ECE) Regulation 13. Uniform provisions concerning the approval of vehicles of categories M, N and O with regard to braking.
34. MIRA. Proving ground - straight line wet grip, <http://www.mira.co.uk/our-services/straight-line-wet-grip> (accessed 10 January 2015)

35. Hunt SW, Odhams AMC, Roebuck RL and Cebon D. Parameter measurement for heavy-vehicle fuel consumption modelling. *Proceedings of the Institution of Mechanical Engineers Part D-Journal of Automobile Engineering*. 2011; 225: 567-89.
36. Bowman D. Assessment of 'R' ratio on SLWG surface. Report, MIRA, UK, 2013.
37. Bevly DM, Parkinson B. Cascaded Kalman filters for accurate estimation of multiple biases, dead-reckoning navigation, and full state feedback control of ground vehicles. *IEEE Transactions on Control Systems Technology*. 2007; 15: 199-208.
38. Morrison G. Combined steering and braking control of articulated heavy goods vehicles. PhD First Year Report, University of Cambridge, UK, 2013.
39. Cheng C. *Enhancing Safety of Actively-Steered Articulated Vehicles*. PhD Thesis, University of Cambridge, UK, 2009.

For access to the raw data used in the production of this paper, please see:

<https://www.repository.cam.ac.uk/handle/1810/248790>